International Journal of Mass Spectrometry 300 (2011) 44–49

Contents lists available at ScienceDirect

International Journal of Mass Spectrometry

journal homepage: www.elsevier.com/locate/ijms

Ion-molecule reactions of $CoAr_6^+$ with di- and trifluorobenzenes probe absolute pressure in FT-ICR MS

Robert F. Höckendorf, Christian van der Linde, O. Petru Balaj, Ina Herber, Martin K. Beyer*

Institut für Physikalische Chemie, Christian-Albrechts-Universität zu Kiel, Olshausenstraße 40, 24098 Kiel, Germany

ARTICLE INFO

Article history:
Received 7 December 2010
Accepted 8 December 2010
Available online 16 December 2010

Keywords:
Gas-phase reactions
Pressure calibration
Rate constant
Ligand exchange
Metal-rare gas complexes

ABSTRACT

A recently introduced pressure calibration scheme with $CoAr_6^+$ as pressure probe agent was reinvestigated with di- and trifluorobenzenes using Fourier transform ion cyclotron resonance (FT-ICR) mass spectrometry. For all reactants ligand exchange was observed as primary reaction. As secondary reactions, ligand exchange and radiative association took place. The results show that pressure calibration for sticky substances is difficult in ultra-high vacuum (UHV), and that ion-molecule reactions which proceed with collision rate are ideal *in situ* pressure probes. A finite-elements simulation of the UHV pressure as a function of time reproduces the experimental findings. The simulation also shows that the actual reactant gas pressure may exhibit significant drift, which is not visible at the pressure gauge.

1. Introduction

In gas phase ion chemistry, an exact measurement of the absolute pressure of reactant gases in ultra-high vacuum (UHV) is required for the determination of absolute rate coefficients, ideally in the location where the reaction takes place, at a pressure of 10^{-10}–10^{-7} mbar. Elaborate schemes for pressure calibration have been developed over the years [1–5]. For Fourier transform ion cyclotron resonance (FT-ICR) mass spectrometry, the empirical correction of the sensitivity of the gauge by Bartmess and Georgiadis [6] in combination with an instrument-specific geometry factor [7,8] is used routinely. This approach is very successful, but problems are encountered for substances with high sticking coefficients [9] at pressures below 10^{-8} mbar. Classic examples of sticky substances with long residence time in vacuum apparatuses are multiply fluorinated benzenes.

For these substances, the pressure calibration factor seems to be pressure dependent, probably because the reactant molecules have a long residence time on the surfaces of the vacuum chamber and the ICR cell: when the needle valve is closed, it takes several minutes before the ion gauge shows a drop in reaction gas pressure, and the base pressure cannot be reached without a thorough bake-out. We therefore apply the recently suggested pressure calibration method [9], using ion molecule reactions that occur with collision rate.

We utilized $CoAr_6^+$ as a pressure probe reactant. Because of the low binding energy of the fifth and sixth argon atom, $CoAr_6^+$ may be expected to react with collision rate with reactants that are significantly more polarizable than argon. Due to its octahedral geometry [10,11], higher-order electric multipole moments are expected to be small. Therefore, its collision rate with polar molecules can be approximated by average dipole orientation (ADO) theory [12–17], in which the ion is described as a point charge. By measuring the rate coefficients of ion-molecule reactions as a function of the nominal pressure shown by the ion gauge, it should be possible to obtain a pressure calibration curve for the reactant of interest.

In our previous work [9], pressure calibration failed for the NO and NO_2 radical, while it worked well with N_2O. Even though NO and NO_2 obviously do not react at collision rate with $CoAr_6^+$, we can still expect the benzene derivatives to do so. Due to their higher mass, higher polarizabilty, larger radius and a long-range cation-π interaction, the binding energy of the collision complex will be higher than the binding energy of an argon atom. Evaporation of argon atoms should therefore be favored over back-dissociation of the collision complex. As soon as vacant coordination sites are available, the di- or trifluorobenzene molecule will coordinate to the Co^+ ion, and the additional energy release will initiate the evaporation of further argon atoms. Also the problem of spin change is eliminated with closed-shell reactants. As a non-sticky test substance, sulfur hexafluoride was chosen for comparison, due to its inert character comparable with molecular nitrogen [18], while shar-

* Corresponding author. Tel.: +49 431 880 2831; fax: +49 431 880 2830.
E-mail address: beyer@phc.uni-kiel.de (M.K. Beyer).

1387-3806/$ – see front matter © 2010 Elsevier B.V. All rights reserved.
doi:10.1016/j.ijms.2010.12.007

ing the high mass and a relatively high polarizability with di- and trifluorobenzenes.

2. Experimental

All mass spectra were taken on a modified Bruker Spectrospin CMS47X mass spectrometer [19–21], equipped with an unshielded 4.7 T superconducting magnet, a Bruker infinity cell, an APEXIII data station, TOPPS ion optics power supply, and an ICC2 Infinity Cell Controller with a BCH preamplifier. The UHV pressure is measured by a radiation shielded IKR020 cold cathode gauge, which is placed above the turbo molecular pump of the cell region.

The ions were produced by laser vaporization of a solid rotating Co disk in an external laser vaporization source [22–24] with a frequency doubled Nd:YAG laser (532 nm, 10 Hz, 5 mJ pulse energy). The metal plasma was entrained in a 50 μs argon gas pulse (22 bar backing pressure, 99.996%) and supersonically expanded into high vacuum, resulting in the formation of $CoAr_n^+$ clusters. The ions were guided by a system of electrostatic lenses into the high field region of the magnet and stored in the ICR cell. $CoAr_6^+$ was mass selected by resonant ejection of unwanted ions. The liquid reactants, all purchased from Sigma–Aldrich, 1,2- (98%), 1,3- (99+%), 1,4-difluorobenzene (≥99%), 1,2,3- (99%), 1,2,4- (98%), 1,3,5-trifluorobenzene (97%) were degassed by three pump–freeze–thaw cycles. The reactant gas SF_6 (Sigma–Aldrich, 99.75+%) was used without further purification. The reaction gases were introduced to the cell region by a needle valve at constant pressure. The temperature of the vacuum chamber was 298 ± 5 K.

The vacuum system of the instrument was optimized for ion-molecule reactions, which require extremely low partial pressures of background gas. In Kiel, the volume of the second chamber was increased, and the turbo molecular pump changed from 150 to 360 L s^{-1}, to reduce gas leakage from the source region to the ultra-high vacuum. The use of laser vaporization with 50 μs gas pulses minimizes the overall gas load in the system, with the pressure in the source chamber going hardly above 10^{-4} mbar during ion generation. Background pressures below 10^{-10} mbar are now routinely reached after bake-out. This low pressure was verified in the experiment with $CoAr_6^+$, where after 10 s no exchange product with background gas, like $Co(H_2O)Ar_n^+$, is visible [9].

To monitor the reactions, mass spectra were taken at different reaction delays and relative reaction rates k_{rel} were obtained by fitting the experimental data assuming pseudo-first-order kinetics. For the kinetic analysis a genetic algorithm [25] implemented in *Analyzze 3.5* [26] was utilized. ADO rates [12–16] were calculated with the *HSA collision rates* program [27,28]. Density functional calculations were performed with the Gaussian 03 [29] program at the B3LYP/6-311++G(3df,3pd) level of theory to obtain polarizabilities α and dipole moments μ_D of the studied species, while the dipole locking constant *c* was taken from literature [12]. The exact values used for calculating ADO rates are given in supporting information, Table SI-1.

3. Results and discussion

3.1. Ion-molecule reactions of $CoAr_6^+$ with di- and trifluorobenzenes

It has already been shown that $CoAr_6^+$ does not fragment due to absorption of black-body infrared radiation [30–38] on the timescale of the present experiment [9]. Since the binding energy of the sixth argon atom is only 10 kJ mol^{-1}, the complexes must be internally colder than room temperature. According to the calculations on the B3LYP/SDD level of theory [9], infrared absorption is inefficient. The major infrared absorbing mode is a triple-degenerate vibration at 118 cm^{-1}, with a calculated intensity of 12 km mol^{-1}. Experimentally, no fragment was observed after storing the mass selected $CoAr_6^+$ for 10 s [9]. Since in the present work, reactions are followed up to 5 s, interference from black-body infrared radiative dissociation can be ruled out.

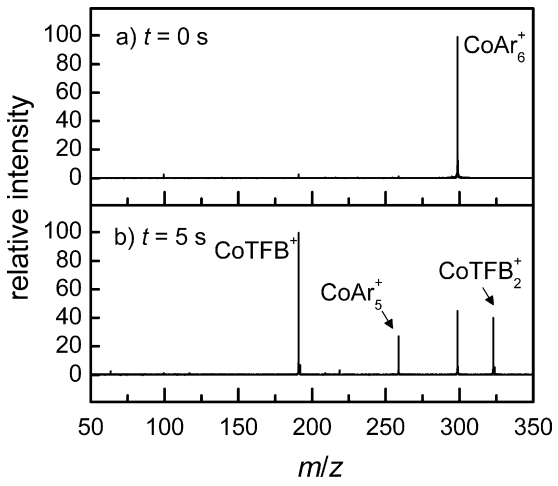

Fig. 1. Mass spectra of the reaction of $CoAr_6^+$ with XFB = **135** at a pressure of 1.6×10^{-8} mbar after (a) 0 s and (b) 5 s reaction delay.

To avoid repetitions, di- and trifluorobenzene isomers are denoted by their substitution pattern only, e.g., **13** stands for 1,3-difluorobenzene, and **124** for 1,2,4-trifluorobenzene. Mass spectra of $CoAr_6^+$ with **135** at 0 s and 5 s reaction delay are shown in Fig. 1.

Ligand exchange in which all six argon atoms are replaced by one XFB molecule, resulting in $CoXFB^+$, is the primary reaction (1) observed for all XFB studied. The mechanism of this reaction is quite straightforward: in the collision complex, the interaction energy of XFB and $CoAr_6^+$ is present largely as vibrational excitation. At a distance of 5 Å, the charge-induced dipole interaction energy already matches the binding energy of the most weakly bound Argon atom, see Fig. SI–1. This causes the evaporation of one or two argon atoms. Now XFB moves to a vacant coordination site, releasing additional energy. This causes the evaporation of the remaining argon atoms. The reaction proceeds close to collision rate, since the first evaporation event of an argon atom will be fast compared to back-dissociation of XFB.

$$CoAr_6^+ + XFB \rightarrow CoXFB^+ + 6Ar \quad (1)$$

As secondary reaction, radiative association [39,40] of a second XFB to $CoXFB^+$ forming $CoXFB_2^+$ takes place, reaction (2).

$$CoXFB + XFB \rightarrow Co(XFB)_2^+ + h\nu \quad (2)$$

A second primary reaction was only observed for **12**, **123** and **124**, the loss of five argon atoms forming the $CoArXFB^+$, reaction (3). Kinetic analysis reveals that the fragmentation of $CoArXFB^+$ to $CoXFB^+$ is pressure dependent, i.e., collision induced, reaction (4). Alternatively, $CoArXFB^+$ may undergo ligand exchange, reaction (5).

$$CoAr_6^+ + XFB \rightarrow CoArXFB^+ + 5Ar, \quad XFB = \mathbf{12}, \mathbf{123}, \mathbf{124} \quad (3)$$

$$CoArXFB^+ + XFB \rightarrow CoXFB^+ + Ar + XFB, \quad XFB = \mathbf{12}, \mathbf{123}, \mathbf{124} \quad (4)$$

$$CoArXFB^+ + XFB \rightarrow Co(XFB)_2^+ + Ar, \quad XFB = \mathbf{12}, \mathbf{123}, \mathbf{124} \quad (5)$$

The collision-induced loss of one argon atom from $CoAr_6^+$ was seen for **123** and **135**, yielding the $CoAr_5^+$ ion, see reaction (6). In a second collision the remaining argon atoms are exchanged against the reactant, reaction (7).

$$CoAr_6^+ + XFB \rightarrow CoAr_5^+ + Ar + XFB, \quad XFB = \mathbf{123}, \mathbf{135} \quad (6)$$

$$CoAr_5^+ + XFB \rightarrow CoXFB^+ + 5Ar, \quad XFB = \mathbf{123}, \mathbf{135} \quad (7)$$

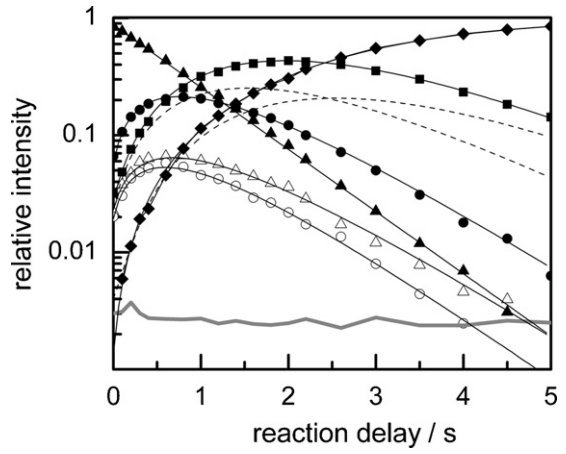

Fig. 2. Kinetics of the reaction of $CoAr_6^+$ with XFB = **123** at a pressure of 3.6×10^{-8} mbar. ▲ $CoAr_6^+$, ■ $CoXFB^+$, ♦ $Co(XFB)_2^+$, ● $CoArXFB^+$, ○ $CoAr_2XFB^+$, Δ $CoAr_5^+$, ▬ noise. Thin solid lines denote pseudo-first-order fit, dashed lines are hot and cold fractions of $CoXFB^+$.

Only for **123**, a ligand exchange of only four argon atoms resulting in the $CoAr_2XFB^+$ complex was observed, reaction (8). This primary product undergoes further fragmentation and/or ligand exchange. Due to the overall low intensity of the intermediates, however, the exact branching ratios of the different pathways could not be determined. Nevertheless, they were included in the fit to account for the observed intensity loss.

$$CoAr_6^+ + XFB \rightarrow CoAr_2XFB^+ + 4Ar, \qquad XFB = \mathbf{123} \tag{8}$$

While the primary reactions are unambiguously extracted from the reaction kinetics, the secondary reactions especially for the trifluorobenzene isomers are not always definitive, due to the large number of possibilities and low product intensities especially in the case of **123**. In Figs. 2 and 3 pseudo-first-order kinetic fits are shown for **123** and **135** in semi-logarithmic plots. The dashed lines in the kinetics symbolize that the freshly formed $CoTFB^+$ has to cool down by infrared radiative cooling [39] or collision before it can take up a second TFB, reaction (2). The $CoTFB^+$ intensity is therefore represented by a hot and a cold fraction. The hot fraction converts to the cold fraction with a first-order rate law. The cold fraction undergoes radiative association of a second TFB.

These experiments also indicate that no significant background of air or water is present in the ultra-high vacuum region, since no exchange products of $CoAr_6^+$ with O_2, H_2O, CO_2 or N_2 are observed.

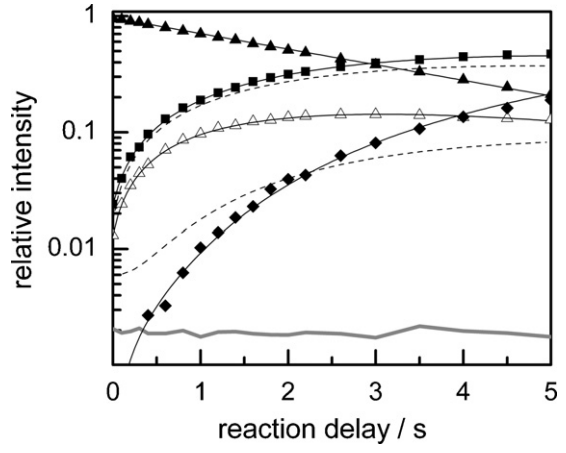

Fig. 3. Kinetics of the reaction of $CoAr_6^+$ with XFB = **135** at a pressure of 1.6×10^{-8} mbar. The black lines are corresponding to the pseudo-first-order fit. ▲ $CoAr_6^+$, ■ $CoXFB^+$, ♦ $Co(XFB)_2^+$, Δ $CoAr_5^+$, ▬ noise. Thin solid lines denote pseudo-first-order fit, dashed lines are hot and cold fractions of $CoXFB^+$.

Table 1
Branching ratios for the primary reactions of $CoAr_6^+$ with the studied fluorobenzene isomers, XFB.

Reaction	**12**	**13**	**14**	**123**	**124**	**135**
(1)	0.35	1.00	1.00	0.05	0.51	0.57
(3)	0.65	–	–	0.54	0.49	–
(6)	–	–	–	0.21	–	0.43
(8)	–	–	–	0.20	–	–

To complete the documentation of the experimental results, branching ratios for the primary reactions of $CoAr_6^+$ are given in Table 1. Obviously, **123** is the most weakly interacting species, with up to two argon atoms remaining after ligand exchange. The ability to knock off an argon atom is correlated with the mass of XFB, which increases the available energy in the collision complex. It would certainly be nice to obtain detailed structural information of $CoXFB^+$ complexes from high-level quantum chemical calculations or spectroscopy. Both tasks are, however, not trivial, and are outside the focus of the present work.

3.2. Pressure calibration

The pressure calibration approach is straightforward and was already described in detail elsewhere [9]. If an ion reacts with collision rate, the calculated collision rate k_{ADO} is equal to the sum of the absolute rate coefficients Σk_{abs} of the observed primary reactions, which in turn depends on the sum of the pseudo-first-order rate coefficients Σk_{rel} and the pressure p_x^{cell}. With this assumption a pressure correction factor K_p for the individual gas at a certain pressure is obtained, Eq. (9). This correction factor replaces the classic calibration factor G/R_x, the geometry factor G [7,8] divided by the ion gauge sensitivity R_x after Bartmess and Georgiadis [6].

$$K_p = \frac{p_x^{cell}}{p_x^{exp}} = \frac{\sum k_{rel} \times k_B \times T}{k_{ADO} \times p_x^{exp}} \tag{9}$$

Here, p_x^{cell} is the actual pressure in the ICR cell, p_x^{exp} is the value read from the sensor, Σk_{rel} [s^{-1}] is the sum of the primary relative rate coefficients, k_{ADO} [$cm^3\ mol^{-1}\ s^{-1}$] is the calculated collision rate, $T = 298 \pm 5$ K the temperature and k_B the Boltzmann constant. The resulting pressure calibration factor can only be as accurate as the calculated collision rate. Since we could not find a statement on the error limits of k_{ADO} in the literature, we use a conservative upper limit of ±10%, based on the experience that efficient reactions of small ions have a rate coefficient close to k_{ADO}.

In Table 2, the pressure correction factors are listed together with the results used to calculate them. For comparison, also the old pressure correction factor, the ratio between the empirical geometry factor G and the sensitivity of the gauge R_x [6,8,9,41] is listed. The experimental results indicate that a pressure calibration curve is needed, since the correction factors K_p listed in Table 2 are pressure dependent. The pressure dependence is most prominent for **14** and **124**. For high pressures the classical pressure calibration is applicable, but it fails for lower pressures. The agreement of both calibration methods in the higher pressure regime indicates that the assumptions are justified.

In our previous study of $CoAr_6^+$ with N_2O and NO, a discrepancy became obvious, since $CoAr_5^+$ reacted 38–91% faster than $CoAr_6^+$. This is a clear sign that $CoAr_6^+$ did not react with collision rate in this case. In the present work, $CoAr_5^+$ is a primary product of the reaction of $CoAr_6^+$ with **123** and **135**. Kinetic analysis shows that the reactivity of $CoAr_5^+$ and $CoAr_6^+$ is the same, within an error limit of 10%, see Table SI-2. This self-consistency of our results indicates that ion-molecule reactions with $CoAr_6^+$ are indeed suitable for pressure calibration of the studied di- and trifluorbenzene isomers.

Table 2
Calculated collision rate coefficients k_{ADO} [10^{-10} cm^3 s^{-1}], sum of the relative rate coefficients Σk_{rel} [s^{-1}] for the primary reactions, measured pressure p_x^{exp} [10^{-8} mbar] and calibrated pressure p_x^{cell} [10^{-8} mbar], newly derived pressure correction factor K_p, and old pressure correction factor G/R_x.

XFB	k_{ADO}	Σk_{rel}	p_x^{exp}	p_x^{cell}	K_p	G/R_x
12	13.50	0.53	2.00	1.61	0.81 ± 0.13	0.8
		0.24	0.80	0.73	0.91 ± 0.12	
		0.19	0.60	0.58	0.96 ± 0.12	
		0.15	0.40	0.46	1.14 ± 0.15	
13	10.80	0.44	2.00	1.68	0.84 ± 0.13	0.8
		0.18	0.80	0.69	0.86 ± 0.10	
		0.14	0.60	0.53	0.89 ± 0.10	
		0.10	0.40	0.38	0.95 ± 0.12	
		0.05	0.20	0.19	0.95 ± 0.14	
14	8.20	0.45	2.00	2.26	1.13 ± 0.17	0.8
		0.19	0.80	0.95	1.19 ± 0.14	
		0.16	0.60	0.80	1.34 ± 0.16	
		0.11	0.40	0.55	1.38 ± 0.17	
		0.06	0.20	0.30	1.50 ± 0.23	
123	13.80	1.21	5.50	3.61	0.66 ± 0.10	0.8
		0.86	4.00	2.56	0.64 ± 0.10	
		0.44	2.00	1.31	0.66 ± 0.11	
		0.20	0.80	0.60	0.75 ± 0.11	
124	10.00	0.65	2.70	2.67	0.99 ± 0.14	0.8
		0.23	0.80	0.95	1.18 ± 0.15	
		0.17	0.60	0.70	1.17 ± 0.15	
		0.13	0.40	0.53	1.34 ± 0.18	
		0.08	0.20	0.33	1.64 ± 0.26	
135	7.90	0.60	4.00	3.12	0.78 ± 0.10	0.8
		0.31	2.00	1.61	0.81 ± 0.13	
		0.14	0.80	0.73	0.91 ± 0.11	
		0.11	0.60	0.57	0.95 ± 0.12	
SF_6	5.80	0.42	2.00	2.98	1.49 ± 0.25	1.4
		0.18	0.80	1.28	1.60 ± 0.22	
		0.11	0.50	0.78	1.56 ± 0.22	

As a further consistency check, we repeated the pressure calibration for SF_6, which does not stick to the cell walls. By evaporating three to five argon atoms, one SF_6 molecule is added to the cluster, reaction (10).

$$CoAr_6^+ + SF_6 \rightarrow CoAr_{6-n}SF_6^+ + nAr \qquad n = 3, 4, 5 \tag{10}$$

As secondary reactions, the fragmentation to the bare $CoSF_6^+$ or the exchange against a second SF_6 molecule, forming $Co(SF_6)_2^+$, was observed.

For sulfur hexafluoride a pressure independent pressure correction factor was obtained, Table 2. The correction factor achieved with the new method K_p and the routinely used method G/R_x agree within experimental error. Since sulfur hexafluoride pumps well, this meets our expectations and completes the picture.

3.3. Pressure dependence of the calibration factor K_p

The pressure dependence of K_p is interesting and disturbing. First of all, possible artifacts have to be ruled out. A potential problem is background gas, especially H_2O, N_2, O_2, and CO_2. No exchange products of these molecules are observed with $CoAr_6^+$, indicating that their concentration is indeed negligible compared to the reactant.

A second argument against a contribution from the background is that its effect would go into the wrong direction: a constant background pressure would become more important with decreasing pressure. At the lowest pressures studied, its contribution would be highest. Consequently, the actual partial pressure of **XFB** would be lower than the apparent value from the pressure gauge. Background would cause a decreasing K_p with decreasing pressure. Experimentally observed is an increasing K_p with decreasing pressure.

It is quite astonishing to see that the pressure dependence of the calibration factor and its magnitude are very sensitive to the substitution patterns of di- and trifluorobenzene. This is seems to be connected to the binding energy of the molecules on the surfaces of the ultra-high vacuum region, especially the ICR cell itself. The Bruker infinity cell is made from gold-plated oxygen free copper, held together by glass ceramics. Close to the ICR cell is a copper seal from the cell flange, and the stainless steel vacuum tubing. Given the wide range of possible adsorption sites, it is impossible to give a detailed, quantitative explanation of the observed effects. There seem to exist particular adsorption properties for fluorobenzenes with two fluorine atoms in *para* position, since the pressure dependence of K_p is most pronounced for **14** and **124**.

3.4. Qualitative numerical simulation of the temporal evolution of UHV pressure

In order to understand these experimental observations, we undertook a numerical simulation of the pressure as a function of time in a one-dimensional model of the vacuum system that captures the essential features, illustrated in Fig. 4. The vacuum system is a tube of L_{Tube} = 2 m length, divided into $n_{segments}$ = 100 segments, the finite volume elements for numerical pressure modeling. The pump is defined as x = 0 m, the pressure sensor is located at x_{sensor} = 0.3 m, the valve at x_{valve} = 1.0 m, and the ICR cell at x_{cell} = 1.9 m. Gas is leaked into the volume segment at x_{valve}. To get the order of magnitude right, we assume a uniform velocity of the gas molecules of 100 m s^{-1}, in positive or negative x direction. We define a probability q_{drift} that in the finite time increment dt of the simulation, a molecule drifts to the neighboring segment:

$$q_{drift} = \frac{n_{segments}}{2\ L_{Tube}} v_x dt \tag{11}$$

The pump is simulated by treating the first segment at x = 0 m as a sink, i.e., molecules can only drift into it, but not back out. The end wall is simulated by allowing drift from the last segment at x = 2 m only to the preceding segment.

If we run a simulation with starting conditions of an empty volume and constant leakage of gas through the valve, the pressure at the sensor and the pressure in the cell quickly become stable, with a pressure-independent geometry factor of x_{valve}/x_{sensor} = 3.33. As expected, change in the leakage through the valve does not affect the geometry factor.

In the next step, we included a high sticking probability in the region of the ICR cell. We defined the number of adsorption sites per segment, and assigned a high number for the segments from x_{cell} to the end of the tube. We assume that adsorption and desorption

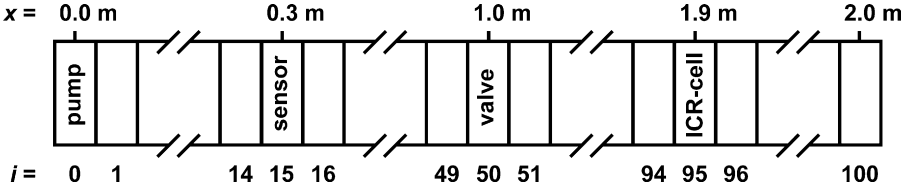

Fig. 4. One-dimensional finite elements model of the vacuum system.

are in equilibrium:

$$N_i^{ad} k_i^{release} = (N_i^{sites} - N_i^{ad}) N_i k_i^{stick} \quad (12)$$

Here, N_i is the number of molecules in segment i in the gas phase, N_i^{ad} is the number of adsorbed molecules, N_i^{sites} is the number of adsorption sites, and $k_i^{release}$, k_i^{stick} are the rate coefficients for release of adsorbed molecules and adsorption of molecules from the gas phase, respectively. We calculated the adsorption–desorption equilibrium for each segment following the drift cycle of the simulation. We also simulated the user operating the leak valve to try to keep the pressure constant. Details of this procedure can be found in the source code of the simulation, which is available as supporting information.

Now the behavior becomes quite complex: as experimentally observed, equilibration of the UHV pressure is delayed. Typical results are shown in Fig. 5. Starting conditions with 25% adsorption sites covered, Fig. 5a, simulate the typical overshoot of the pressure after opening the valve with a sticky substance. After the sensor shows that gas is leaking in, the valve is closed again a little bit, and the user waits for the pressure to equilibrate to the desired value. In order to keep the pressure constant, the user has to increase the gas flow from time to time, shown by the steps in the sensor curve. This is quite reasonable, since the cell region serves as a source of gas, and is slowly evacuated by the pressure gradient. Stable conditions are reached when the geometry factor reaches its default value of 3.33, coming from an initial value of 4.06. In Fig. 5b, the simulation starts with a clean UHV. The user slowly opens the valve, until the desired pressure is reached. Here the cell region acts as a sink for the sticky gas. Once the surfaces are significantly covered, an ever smaller gas flow is sufficient to maintain the desired pressure at the sensor. The pressure reading suggests a very satisfactory stability of the pressure. In the cell region, however, the pressure increases, and the geometry factor changes from close to 0 to 3.33.

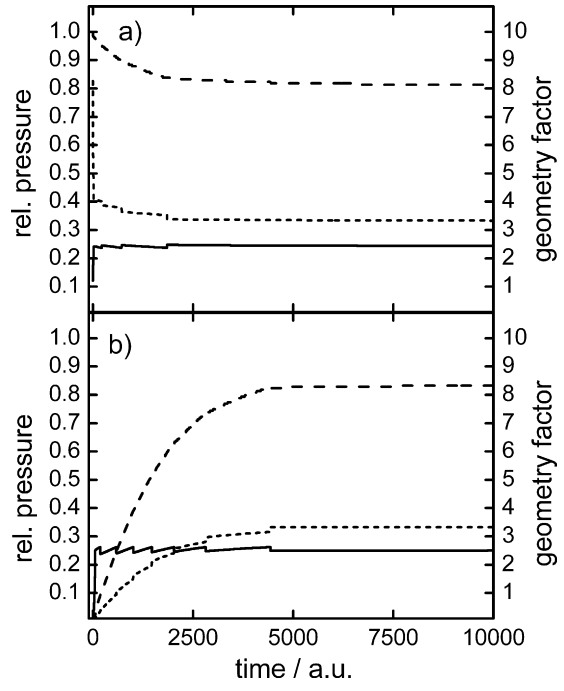

Fig. 5. Numerical simulation of the pressure in the vacuum system as a function of time for the pressure in the ICR cell (long dash line), the sensor pressure (straight line) and the resulting geometry factor (short dash line. (a) starting with 25% coverage of adsorption. (b) Starting with 0% coverage.

3.5. Consequences for ion-molecule reaction studies with sticky substances

The simulations clearly show that for any sticky gas, the actual pressure in the ICR cell may drift significantly during an experiment, even though the user manages to keep the sensor reading constant. The frequency of user interference is directly correlated to the stability of the actual pressure: The longer the periods between adjustments at the needle valve, the more stable the pressure in the ICR cell. The simulation also suggests that pressure drift is smaller if the desired pressure is approached from higher values, like in Fig. 5a, while a very careful opening of the leak valve may lead to the more severe drift problems shown in Fig. 5b.

The obvious recommendation is to be patient and wait for the pressure to reach a stable value. This becomes, however, more and more difficult going to lower pressures. In experiments where low pressures are desirable, like nanocalorimetry [42,43], it may simply take too long to reach stationary conditions. Depending on the adsorption/desorption kinetics, reaching ideal conditions may take minutes, hours, or days. However, as long as the pressure drift is small on the time scale of the complete kinetics experiment, it does not adversely affect the results. This is the regime in which the current experiments have been done.

A hidden drift of actual pressure in the ICR cell, as evidenced in the simulation, may also account for the puzzling isomer effects observed with sticky substances. In recent experiments of gold anions with trifluoroacetic acid [44], an increase of reactivity with time was observed, interpreted as a collisional cooling effect of the reactant. A pressure drift like in the simulation of Fig. 5b, however, would have a similar effect.

4. Conclusions

In line with previous studies of argon solvated metal clusters [9,45–47], ligand exchange was the primary reaction with $CoAr_6^+$ for all studied reactants, in part accompanied by collision induced loss of one argon atom. The experimental results combined with the numerical simulation show that for sticky substances like di- and trifluorobenzene isomers, the classical calibration method may fail at very low pressures, because the stationary state described with the substance-independent geometry factor may not be reached on the timescale of the experiment. Especially in the pressure regime below 10^{-8} mbar, the calibration factor may become strongly pressure-dependent for sticky substances, and significant drift of the actual reactant gas pressure may occur.

Acknowledgements

Financial support from the Deutsche Forschungsgemeinschaft and the Fonds der Chemischen Industrie is gratefully acknowledged.

Appendix A. Supplementary data

Supplementary data associated with this article can be found, in the online version, at doi:10.1016/j.ijms.2010.12.007.

References

[1] R.L. Summers, NASA Report TN D-5285, 1969.
[2] T.A. Flaim, P.D. Ownby, J. Vacuum Sci. Technol. 5 (1971) 661.
[3] R. Holanda, NASA Report TN D-6815, 1972.
[4] M. Schulte, B. Schlosser, W. Seidel, Fresen. J. Anal. Chem. 348 (1994) 778.
[5] F. Nakao, Vacuum 25 (1975) 431.
[6] J.E. Bartmess, R.M. Georgiadis, Vacuum 33 (1983) 149.
[7] M.L. Anderson, M.S. Ford, P.J. Derrick, T. Drewello, D.P. Woodruff, S.R. Mackenzie, J. Phys. Chem. A 110 (2006) 10992.

[8] T. Schindler, C. Berg, G. Niedner-Schatteburg, V.E. Bondybey, Ber. Bunsen-Ges. Phys. Chem 96 (1992) 1114.
[9] C. van der Linde, R.F. Höckendorf, O.P. Balaj, M.K. Beyer, Low Temp. Phys. 36 (2010) 411.
[10] M. Beyer, C. Berg, G. Albert, U. Achatz, V.E. Bondybey, Chem. Phys. Lett. 280 (1997) 459.
[11] D. Lessen, P.J. Brucat, Chem. Phys. Lett. 149 (1988) 10.
[12] L. Bass, T. Su, M.T. Bowers, Int. J. Mass Spectrom. Ion Process. 28 (1978) 389.
[13] L. Bass, T. Su, W.J. Chesnavich, M.T. Bowers, Chem. Phys. Lett. 34 (1975) 119.
[14] T. Su, M.T. Bowers, J. Chem. Phys. 58 (1973) 3027.
[15] T. Su, M.T. Bowers, Int. J. Mass. Spectrom. Ion Phys. 12 (1973) 347.
[16] T. Su, E.C.F. Su, M.T. Bowers, J. Chem. Phys. 69 (1978) 2243.
[17] P. Langevin, Ann. Chim. Phys. 5 (1905) 245.
[18] N. Wiberg, A.F. Holleman:, Lehrbuch der Anorganischen Chemie, Walter de Gruyter & Co, Berlin, 1995.
[19] M. Allemann, H. Kellerhals, K.P. Wanczek, Int. J. Mass Spectrom. Ion Process. 46 (1983) 139.
[20] P. Kofel, M. Allemann, H. Kellerhals, K.P. Wanczek, Int. J. Mass Spectrom. Ion Process. 72 (1986) 53.
[21] C. Berg, T. Schindler, G. Niedner-Schatteburg, V.E. Bondybey, J. Chem. Phys. 102 (1995) 4870.
[22] S. Maruyama, L.R. Anderson, R.E. Smalley, Rev. Sci. Instrum. 61 (1990) 3686.
[23] T.G. Dietz, M.A. Duncan, D.E. Powers, R.E. Smalley, J. Chem. Phys. 74 (1981) 6511.
[24] V.E. Bondybey, J.H. English, J. Chem. Phys. 74 (1981) 6978.
[25] D.E. Goldberg, Gentic Algorithms in Search, Optimization & Machine Learning, Addison-Wesley, Massachusetts, 1989.
[26] M.K. Beyer, Analyzze 3.5, Christian-Albrechts-Universität zu Kiel, Technische Universität Berlin und Technische Universität München, 2010.
[27] M.K. Beyer, HSA collision rates vs. 2.0, Technische Universität München, 2005.
[28] G. Kummerlöwe, M.K. Beyer, Int. J. Mass Spectrom. 244 (2005) 84.
[29] M.J. Frisch, G.W. Trucks, H.B. Schlegel, et al., Gaussian 03, Revision C.02, Gaussian, Inc., Wallingford, CT, 2004.
[30] R.C. Dunbar, T.B. McMahon, Science 279 (1998) 194.
[31] R.C. Dunbar, Mass Spectrom. Rev. 23 (2004) 127.
[32] B.S. Fox, M.K. Beyer, V.E. Bondybey, J. Phys. Chem. A 105 (2001) 6386.
[33] P.D. Schnier, W.D. Price, R.A. Jockusch, E.R. Williams, J. Am. Chem. Soc. 118 (1996) 7178.
[34] P. Weis, O. Hampe, S. Gilb, M.M. Kappes, Chem. Phys. Lett. 321 (2000) 426.
[35] T. Schindler, C. Berg, G. Niedner-Schatteburg, V.E. Bondybey, Chem. Phys. Lett. 250 (1996) 301.
[36] D. Thölmann, D.S. Tonner, T.B. McMahon, J. Phys. Chem. 98 (1994) 2002.
[37] E.N. Kitova, D.R. Bundle, J.S. Klassen, J. Am. Chem. Soc. 124 (2002) 5902.
[38] M. Sena, J.M. Riveros, Rapid Commun. Mass Spectrom. 8 (1994) 1031.
[39] R.C. Dunbar, Mass Spectrom. Rev. 11 (1992) 309.
[40] S.J. Klippenstein, Y.C. Yang, V. Ryzhov, R.C. Dunbar, J. Chem. Phys. 104 (1996) 4502.
[41] D. Schröder, H. Schwarz, D.E. Clemmer, Y.M. Chen, P.B. Armentrout, V.I. Baranov, D.K. Bohme, Int. J. Mass Spectrom. Ion Process. 161 (1997) 175.
[42] R.F. Höckendorf, C. van der Linde, O.P. Balaj, M.K. Beyer, Phys. Chem. Chem. Phys. 12 (2010) 3772.
[43] R.F. Höckendorf, C.-K. Siu, C. van der Linde, O.P. Balaj, M.K. Beyer, Angew. Chem. Int. Ed. 49 (2010) 8257.
[44] R.F. Höckendorf, Y.L. Cao, M.K. Beyer, Organometallics 29 (2010) 3001.
[45] G. Albert, C. Berg, M. Beyer, U. Achatz, S. Joos, G. Niedner-Schatteburg, V.E. Bondybey, Chem. Phys. Lett. 268 (1997) 235.
[46] V.E. Bondybey, M.K. Beyer, J. Phys. Chem. A 105 (2001) 951.
[47] U. Achatz, M. Beyer, S. Joos, B.S. Fox, G. Niedner-Schatteburg, V.E. Bondybey, J. Phys. Chem. A 103 (1999) 8200.